

Implications of advanced collision operators for gyrokinetic simulation

E A Belli and J Candy

General Atomics, P.O. Box 85608, San Diego, CA 92186-5608, USA

E-mail: bellie@fusion.gat.com

Abstract. In this work, we explore both the potential improvements and pitfalls that arise when using advanced collision models in gyrokinetic simulations of plasma microinstabilities. Comparisons are made between the simple-but-standard electron Lorentz operator and specific variations of the advanced Sugama operator. The Sugama operator describes multi-species collisions including energy diffusion, momentum and energy conservation terms, and is valid for arbitrary wavelength. We report scans over collision frequency for both low and high $k_\theta \rho_s$ modes, with relevance for multi-scale simulations that couple ion and electron scale physics. The influence of the ion-ion collision terms – not retained in the electron Lorentz model – on the damping of zonal flows is also explored. Collision frequency scans for linear and nonlinear simulations of ion-temperature-gradient instabilities including impurity ions are presented. Finally, implications for modeling turbulence in the highly-collisional edge are discussed.

1. Introduction

For gyrokinetic studies of plasma microturbulence in the tokamak pedestal, accurate treatment of collisions is a potential concern because of the relatively large normalized collision frequencies. For example, in the DIII-D core, the normalized collision rate $\bar{\nu}_e = (a/c_s)\tau_{ee}^{-1}$ is small – typically $\bar{\nu}_e \ll 1$ – whereas in the pedestal $\bar{\nu}_e > 1$. Collisions can be important in gyrokinetics since electron collisions damp linear drift modes through electron detrapping [1, 2, 3], while ion-ion collisions can damp the stabilizing zonal flows [4].

To more accurately treat the collisional regime, a new gyrokinetic solver (CGYRO) has been developed for more precise studies of high-collisionality plasma regimes [5]. Building on the neoclassical code NEO [6, 7], CGYRO adopts the NEO pitch angle and energy velocity-space coordinate system (ξ, ε) (where $\xi = v_\parallel/v$ and $\varepsilon = v^2/2$) to simplify the numerical discretization of the collision operator and optimize the associated accuracy. This allows for the accurate discretization of complex operators that retain important inter-species momentum and energy exchange terms. Existing gyrokinetic codes, developed at a time when collisionless simulations were the focus, typically use a numerical mesh optimized for the collisionless equations (see figure 1

of Ref. [5]). CGYRO takes a different approach and optimizes the discretization for the collisional limit. In addition, most prior gyrokinetic studies have included only simple Lorentz pitch-angle scattering. While advanced operators including energy diffusion have recently been implemented in GS2 [8], GENE [9], and GKW [10], the discretizations were carried out using the legacy coordinates and numerical meshes. In the literature, systematic discussion of the implications of, and subtleties associated with, using advanced operators is scant. With GS2, it was shown in simplified Z-pinch geometry that energy diffusion suppresses the short wavelength structure beyond that due to pitch angle scattering alone [8]. Some detailed studies in tokamak geometry were recently done with GKW, showing that energy diffusion enhances the stabilization of trapped electron modes (TEM) [10]. In this work, we extend the discussion to provide a more comprehensive study of these effects, using new numerical methods suitable for the collisional limit.

The rest of this paper is organized as follows. In section 2, the basic simulation model, including the collision models, is described. Numerical results are presented in section 3, including a comparison of reduced collision models on gyrokinetic linear stability and nonlinear turbulence. Finally, a brief summary is given in section 4.

2. Simulation Model

CGYRO solves the nonlinear, electromagnetic gyrokinetic equations [11, 12] in (ξ, u_a) velocity-space coordinates. Here the velocity-space coordinates are the cosine of the pitch angle, $\xi \doteq v_{\parallel}/v$, and the normalized velocity, $u_a = v/(\sqrt{2}v_{ta})$ where a is the species label. The numerical algorithm is described in detail in Ref. [5]. The code is pseudospectral in the velocity dimensions and fully spectral in the radial and binormal directions. CGYRO treats electrons and all ion species gyrokinetically for arbitrary wavelength. Flux surfaces can have arbitrary shape and, by virtue of the Miller equilibrium formulation, are consistent with an exact Grad-Shafranov equilibrium [13]. Both transverse and compressional electromagnetic fluctuations are included, and $\mathbf{E} \times \mathbf{B}$ shear, parallel velocity shear, and finite-mach-number terms are retained in a manner consistent with GYRO [14].

2.1. Units, Conventions, and Definitions

Unless otherwise specified, the following units and conventions are used throughout this paper. We define a spatial coordinate r which measures the half-width of the flux-surface at the elevation of the centroid [13]. For brevity, we will refer to this as the *minor radius*, although a more descriptive name is the *midplane minor radius*. It has dimensions of length, and for an up-down symmetric circular flux-surface, r is just the usual circular minor radius. Length is measured in units of a , the value of r at the last closed flux surface. The *inverse aspect ratio* is $\epsilon = r/R_0$, where R_0 is the *midplane major radius* of the flux surface. Frequencies are measured in units of c_s/a , where $c_s = \sqrt{T_e/m_D}$ is the

deuteron sound speed, T_e is the electron temperature, and m_D is the deuteron mass. It is also useful to define the species-dependent thermal speed as $v_{ta} = \sqrt{T_a/m_a}$, where subscript a denotes the species index.

Next we introduce an *effective magnetic field* B_{unit} [13, 15], which is defined with reference to a global equilibrium through the relation

$$B_{\text{unit}} = \frac{q}{r} \frac{\partial \psi}{\partial r}, \quad (1)$$

where q is the safety factor and ψ is the poloidal flux divided by 2π . Unlike the field strength $B(\psi, \theta)$, the effective field B_{unit} is constant on a flux surface. In terms of B_{unit} , we define an effective *ion-sound gyroradius* as

$$\rho_s \doteq \frac{c_s}{eB_{\text{unit}}/(m_D c)}. \quad (2)$$

For nonlinear simulations, because the particle and energy fluxes have a natural gyroBohm scaling, we normalize them to a reference gyroBohm level,

$$\Gamma_{GB} = n_e c_s \rho_*^2 \quad \text{and} \quad Q_{GB} = n_e T_e c_s \rho_*^2, \quad (3)$$

where $\rho_* \doteq \rho_s/a$. The effective electron beta and the effective pressure gradient are defined as

$$\beta_{e,\text{unit}} \doteq \frac{8\pi n_e T_e}{B_{\text{unit}}^2} \quad \text{and} \quad \beta_* = -\frac{8\pi}{B_{\text{unit}}^2} \frac{dp}{dr}, \quad (4)$$

where $p = \sum_a n_a T_a$ is the total plasma pressure. The species-dependent temperature and density gradient scale lengths are written as $1/L_{T_a} = -d \ln T_a / dr$ and $1/L_{n_a} = -d \ln n_a / dr$. Note that, although $\beta_{e,\text{unit}}$, β_* , and the density and temperature profiles are related, they can be varied independently for theoretical investigation. Specifically, $\beta_{e,\text{unit}}$ enters the gyrokinetic equation through the gyrokinetic-Ampère equation and affects the strength of the magnetic fluctuations (see Eq. (68) in Ref. [5]), whereas β_* is used to determine the effect of the plasma pressure gradient on the equilibrium [16]. Thus, varying β_* at fixed $\beta_{e,\text{unit}}$ and $1/L_{T_a}$ and $1/L_{n_a}$ isolates the geometric pressure gradient effect without affecting the relative magnitudes of the magnetic fluctuations and the diamagnetic drifts.

Finally, the inter-species collision rates are given by

$$\tau_{ab}^{-1} = \frac{\sqrt{2}\pi e^4 z_a^2 z_b^2 n_b}{m_a^{1/2} T_a^{3/2}} \ln \Lambda. \quad (5)$$

For parameter scans, rather than the a - b collision rate above, it is useful to introduce the dimensionless electron collision frequency,

$$\bar{\nu}_e = \frac{a}{c_s} \tau_{ee}^{-1} = \frac{a}{c_s} \frac{\sqrt{2}\pi e^4 n_e}{m_e^{1/2} T_e^{3/2}} \ln \Lambda. \quad (6)$$

2.2. General expression of the gyroaveraged collision operator

The linearized gyrophase-averaged collision operator can be written as

$$C_{ab}^{\text{GK}} \doteq \sum_{\mathbf{k}_\perp} \oint \frac{d\vartheta}{2\pi} e^{iS(\mathbf{R})} e^{i\mathbf{k}_\perp \cdot \boldsymbol{\rho}_a} C_{ab}^L(f_{1a, \mathbf{k}_\perp}, f_{1b, \mathbf{k}_\perp}), \quad (7)$$

where \mathbf{R} is the position of the guiding center, ϑ is the gyroangle, and $\boldsymbol{\rho}_a = \boldsymbol{\rho}_a(\vartheta)$ is the gyroradius vector. The perpendicular wavenumber is given by $\mathbf{k}_\perp \doteq \nabla_\perp S$. In this notation, the fluctuating part of the perturbed particle distribution takes the form

$$f_{1a}(\mathbf{R}, \xi, u_a) = \sum_{\mathbf{k}_\perp} e^{iS(\mathbf{R})} f_{1a, \mathbf{k}_\perp}(\xi, u_a), \quad (8)$$

where each spectral component is the sum of a gyroangle-independent term and a gyroharmonic term:

$$f_{1a, \mathbf{k}_\perp} \doteq -\frac{z_a e f_{0a}}{T_a} \delta\phi_{\mathbf{k}_\perp} + e^{-i\mathbf{k}_\perp \cdot \boldsymbol{\rho}_a} H_{a, \mathbf{k}_\perp}. \quad (9)$$

Here $\delta\phi_{\mathbf{k}_\perp}$ is the fluctuating electrostatic potential and H_{a, \mathbf{k}_\perp} is the non-adiabatic distribution. The general linearized collision operator is separated into a *test particle* component C_{ab}^T and a *field particle* component C_{ab}^F , such that

$$C_{ab}^L(H_{a, \mathbf{k}_\perp}, H_{b, \mathbf{k}_\perp}) = C_{ab}^T(H_{a, \mathbf{k}_\perp}) + C_{ab}^F(H_{b, \mathbf{k}_\perp}). \quad (10)$$

In this work, we consider two models for C_{ab}^L : the simple Lorentz operator and the advanced Sugama operator.

2.3. The Sugama collision operator

The recently-developed *Sugama operator* [17] is a sophisticated approximation to the full linearized, gyroaveraged Fokker-Planck operator. It is designed to conserve particles, momentum, and energy, and to satisfy adjointness relations and Boltzmann's H-theorem. Compared with the operator of Abel *et al.* [18], the Sugama operator, extends the regime of validity to include the description of unlike-species collisions, including those with different temperatures $T_a \neq T_b$.

The test-particle component of the Sugama operator [17] is actually the full, unmodified linearized gyroaveraged Fokker-Planck test-particle operator (pitch-angle scattering plus diffusion). This is written as

$$C_{ab}^T(H_{a, \mathbf{k}_\perp}) = C_{ab}^{T0}(H_{a, \mathbf{k}_\perp}) - H_{a, \mathbf{k}_\perp} k_\perp^2 \rho_a^2 \frac{u_a^2}{2} \left[\nu_{ab}^D (1 + \xi^2) + \nu_{ab}^\parallel (1 - \xi^2) \right], \quad (11)$$

and is valid at arbitrary wavelength. For the case of like-species and inter-ion species collisions (for which we assume $T_a = T_b$),

$$C_{ab}^{T0}(H_{a, \mathbf{k}_\perp}) = \nu_{ab}^D \mathcal{L} H_{a, \mathbf{k}_\perp} + \mathcal{D}(H_{a, \mathbf{k}_\perp}). \quad (12)$$

In the ion-electron and electron-ion parts of the operator, we neglect terms which are $\mathcal{O}(m_e/m_i)$ smaller than the dominant (electron) collision terms. Because $m_e/m_D <$

3×10^{-4} , these terms are potentially smaller than the nominal truncation error and for this reason it is justifiable to neglect them. Thus, we have

$$C_{ie}^{T0}(H_{i,\mathbf{k}_\perp}) = 0 \quad \text{and} \quad C_{ei}^{T0}(H_{e,\mathbf{k}_\perp}) = \nu_{ei}^D \mathcal{L} H_{e,\mathbf{k}_\perp} . \quad (13)$$

In Eqs. (12) and (13), \mathcal{L} is the Lorentz (pitch-angle scattering) operator,

$$\mathcal{L} = \frac{1}{2} \frac{\partial}{\partial \xi} (1 - \xi^2) \frac{\partial}{\partial \xi} , \quad (14)$$

and \mathcal{D} is the diffusion operator,

$$\mathcal{D}_{ab}(H_{a,\mathbf{k}_\perp}) = \frac{1}{u_a^2} \frac{\partial}{\partial u_a} \left[\nu_{ab}^{\parallel} \left(\frac{1}{2} u_a^4 \frac{\partial H_{a,\mathbf{k}_\perp}}{\partial u_a} + \frac{T_a}{T_b} u_a^5 H_{a,\mathbf{k}_\perp} \right) \right] , \quad (15)$$

where the pitch-angle diffusion (deflection) rate ν^D is

$$\nu_{ab}^D(v) = \frac{\tau_{ab}^{-1}}{u_a^3} \left[\frac{1}{\sqrt{\pi} u_b} e^{-u_b^2} + \text{erf}(u_b) \left(1 - \frac{1}{2u_b^2} \right) \right] , \quad (16)$$

and the parallel velocity diffusion rate ν^{\parallel} is

$$\nu_{ab}^{\parallel}(v) = 2 \frac{\tau_{ab}^{-1}}{u_a^3} \left[-\frac{1}{\sqrt{\pi} u_b} e^{-u_b^2} + \text{erf}(u_b) \left(\frac{1}{2u_b^2} \right) \right] . \quad (17)$$

The field particle component of the Sugama operator is ad hoc, designed to conserve momentum and energy, i.e.,

$$C_{ab}^F(H_{b,\mathbf{k}_\perp}) = R_{ab}^M + R_{ab}^E , \quad (18)$$

where

$$R_{ab}^M = \eta_{ab}^M \left[J_0(\gamma_a) \int d^3v J_0(\gamma_b) \frac{H_{b,\mathbf{k}_\perp}}{f_{0b}} C_{ba}^{T0}(v_{\parallel} f_{0b}) \right. \\ \left. + J_1(\gamma_a) \frac{v_{\perp}}{v_{\parallel}} \int d^3v J_1(\gamma_b) \frac{v_{\perp}}{v_{\parallel}} \frac{H_{b,\mathbf{k}_\perp}}{f_{0b}} C_{ba}^{T0}(v_{\parallel} f_{0b}) \right] , \quad (19)$$

$$R_{ab}^E = \eta_{ab}^E J_0(\gamma_a) \int d^3v J_0(\gamma_b) \frac{H_{b,\mathbf{k}_\perp}}{f_{0b}} C_{ba}^{T0}(u_b^2 f_{0b}) . \quad (20)$$

Above, we have defined

$$\eta_{ab}^M \doteq -\frac{m_b}{m_a} \frac{C_{ab}^{T0}(v_{\parallel} f_{0a})}{\int d^3v v_{\parallel} C_{ab}^{T0}(v_{\parallel} f_{0a})} , \quad (21)$$

$$\eta_{ab}^E \doteq -\frac{T_b}{T_a} \frac{C_{ab}^{T0}(u_a^2 f_{0a})}{\int d^3v u_a^2 C_{ab}^{T0}(u_a^2 f_{0a})} . \quad (22)$$

2.4. The Lorentz electron collision operator

The simple *Lorentz operator* is implemented in most gyrokinetic codes. It retains only the essential pitch-angle scattering dynamics and can be written as

$$C_{ee}^L = \nu_{ee}^D \mathcal{L} H_{e,\mathbf{k}_\perp} , \quad (23)$$

$$C_{ei}^L = \frac{\tau_{ei}^{-1}}{u_a^3} \mathcal{L} H_{e,\mathbf{k}_\perp} , \quad (24)$$

$$C_{ii}^L = C_{ie}^L = 0 . \quad (25)$$

It employs the small electron-to-ion mass ratio approximation, ignoring terms of $\mathcal{O}(m_e/m_i)^{1/2}$ and smaller. Because it neglects the field particle component for all species, the Lorentz model is *not* momentum conserving. Despite its simplicity, simulation results show that the model is nevertheless relatively accurate for core plasmas. The physical explanation for the accuracy is related to the collisionless discontinuity at the electron trapped-passing (TP) boundary layer. At finite but small $\bar{\nu}_e \rightarrow 0$, the discontinuity is resolved by collisions and a boundary-layer ordering shows that the collision operator is asymptotically dominated by the term $\partial^2 H_{a,\mathbf{k}_\perp} / \partial \xi^2$ [19].

3. Simulations based on the GA Standard Case

A comparison of collision models is made for various linear toroidal drift waves: ion-temperature-gradient (ITG) mode, trapped-electron mode (TEM), kinetic-ballooning mode (KBM), and electron-temperature-gradient mode (ETG). The comparisons also explore effects on the residual zonal potential as well as on nonlinear turbulence. For ITG test case parameters, we use the General Atomics (GA) standard case parameters [20]: $R_0/a=3$, $r/a=0.5$, $q=2$, $T_i=T_e$, $a/L_{ni}=a/L_{ne}=1$, $a/L_{Ti}=a/L_{Te}=3$. For the geometry we use an unshifted Miller circular equilibrium [21, 22]. It is important to note that this *not* a model equilibrium; on the contrary, it is a very-high-precision numerical solution of the Grad-Shafranov equation on the flux-surface of interest. We consider fixed $k_\theta \rho_s = 0.3$. ITG results with the Lorentz collision operator have been previously benchmarked with GYRO [5]. For the other modes we have the following variations:

- For KBM test case parameters, we additionally set $\beta_{e,\text{unit}}=0.7\%$ (with $\beta_*=0$).
- For TEM test case parameters, we modify only the ion temperature gradient such that $a/L_{Ti}=1.0$.
- For ETG test case parameters, we consider fixed $k_\theta \rho_s=18$.

3.1. Impact of collisions on linear drift-waves

A comparison of the Lorentz and Sugama collision models is shown in figures 1-4 for the ITG, TEM, KBM, and ETG test cases. Since both the ITG and TEM modes are destabilized by the trapped electron population, it is not surprising that both are stabilized by collisions, particularly in the weak-collision regime $\bar{\nu}_e < 1$. This is consistent with the interpretation that Lorentz collisions cause detrapping of trapped electrons. Because the TEM – unlike the ITG – does not exist in the absence of trapped electrons, it is also unsurprising that the TEM is most strongly stabilized by collisions. On the other hand, the KBM and ETG mode are only weakly affected by collisions – particularly at low $\bar{\nu}_e$. For these latter modes, a physical interpretation of the effect of collisions is more difficult because the main effect occurs in the regime for which Lorentz collisions no longer dominate the dynamics. While Lorentz collisions are weakly *destabilizing* for both modes, interpretation of the general results for the KBM and ETG mode must be discussed separately.

An important feature of the curves in figures 1-4 is to clearly illustrate the differences between various collision models. Our results show that the simple Lorentz operator agrees well with the full Sugama operator, for all modes, at low collision frequency ($\bar{\nu}_e < 1$). Furthermore, the agreement becomes exceptional in the range $\bar{\nu}_e < 0.1$. As noted already, the mode most sensitive to the collision model is the TEM (see figure 2). Here we find that the Lorentz model can underestimate the stabilization and thus overestimate the TEM growth rate. We note that the observation of enhanced stabilization of the TEM with the Sugama model, primarily due to the energy diffusion, is consistent with earlier results from GKW [10]. We can summarize the results quantitatively: the error in the magnitude of the frequency is lowest for the KBM, staying below 2% across the entire range. The error is largest for the TEM, reaching 6% by $\bar{\nu}_e=0.1$ and up to 17% by $\bar{\nu}_e=1$. The error for the ITG mode is a low 1% by $\bar{\nu}_e=0.1$, increasing up to 3.5% by $\bar{\nu}_e=1$ and 7% by $\bar{\nu}_e=10$. In the pedestal, where $\bar{\nu}_e \sim 1$, these results suggest that advanced collision models like the Sugama operator are needed for accurately modeling the TEM and ITG stability. Like the KBM case, the error in the Lorentz model for the ETG mode is low, specifically 0.02% by $\bar{\nu}_e=0.1$, increasing up to 0.09% by $\bar{\nu}_e=1$ and 3% by $\bar{\nu}_e=10$. However, the trend for the growth rate and the real frequency with $\bar{\nu}_e$ for the Lorentz operator is incorrect, with the Lorentz model destabilizing the mode and the full Sugama model stabilizing the mode. Comparison with the Sugama model neglecting FLR terms (green curve) demonstrates that this difference is primarily due to the FLR collisional effects. This will be discussed further below.

For the Sugama model, the effects of the momentum and energy restoring terms were also examined independently. Neglecting the momentum restoring term ($R^M=0$) had only a relatively slight effect on the frequency at low collisionality ($< 0.3\%$ for the ITG mode and KBM and 1% for the TEM by $\bar{\nu}_e=0.1$, growing to 3% for the ITG mode and KBM and 6% for the TEM by $\bar{\nu}_e=1$). However, this grew by a factor of 3-5 when neglecting the energy restoring term ($R^E=0$). This was most significant for the TEM, consistent with previous GKW results [10]. Perhaps the most important conclusion of these linear results is related to the proper implementation of energy conservation. Lack of energy conservation leads to a significant overdamping of the ITG and TEM. In fact, here we find that the TEM is completely stabilized by $\bar{\nu}_e=0.1$, rather than by $\bar{\nu}_e=1.0$, if energy conservation is not implemented in the full operator. For this reason, we claim that energy conservation is essential in any advanced collision model. Or, to put it another way, it is a mistake to implement (say) energy diffusion in a gyrokinetic collision operator if the implementation is not energy conserving.

Finite-Larmor-radius (FLR) terms in the Sugama model have also been studied. Unsurprisingly, only exceptionally small differences were found when including these terms for the low- $k_\theta \rho_s$ test cases. For example, for the TEM and KBM, the error in neglecting FLR terms ($k_\perp=0$) was less than 0.1%. For the ITG mode, where ion dynamics are more dominant and thus k_\perp effects stronger, the error was still less than 1% up to $\bar{\nu}_e=2.0$. This indicates that much of the difference between the

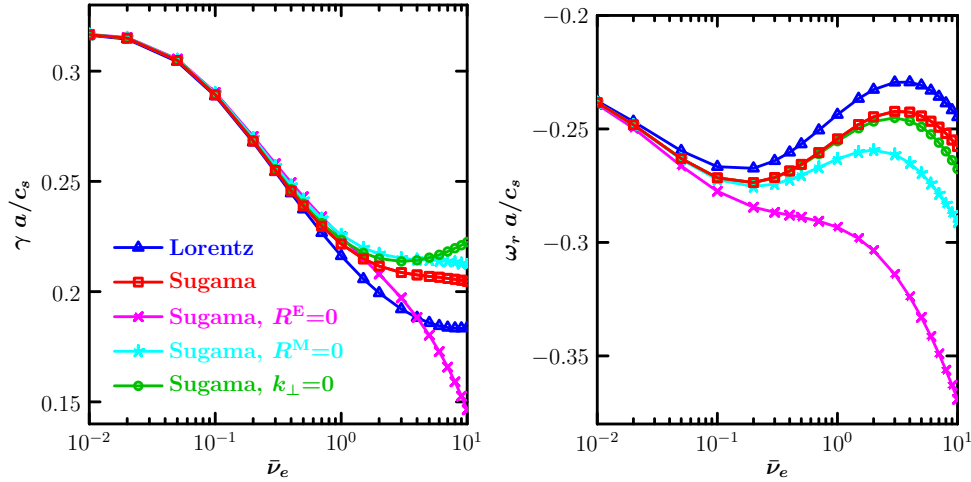


Figure 1. Linear growth rate γ and real frequency ω_r versus collision rate $\bar{\nu}_e$ for an ITG mode. Results from the Lorentz collision model are compared with the Sugama model. In the legend, $R^E=0$ means that energy conserving terms are ignored in C^F , $R^M=0$ means that momentum conserving terms are ignored in C^F , and $k_\perp=0$ means all FLR terms are ignored in C^L .

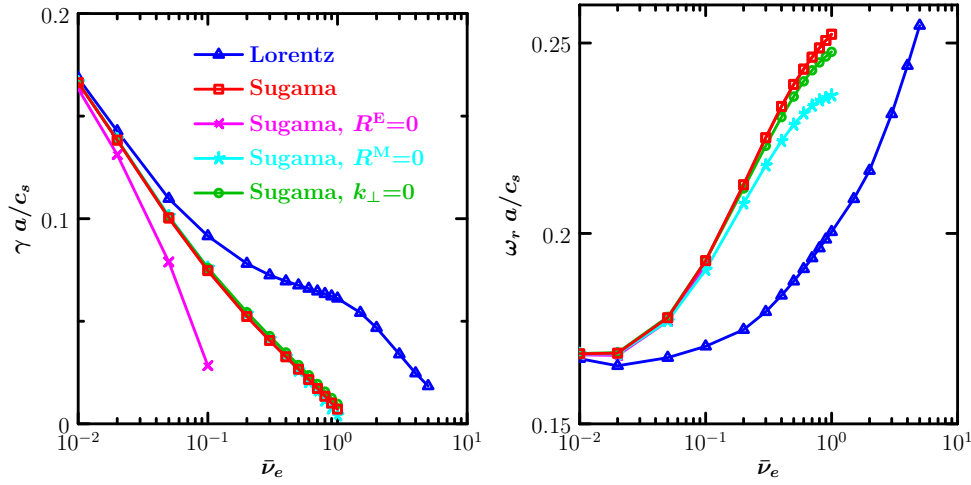


Figure 2. Linear growth rate γ and real frequency ω_r versus collision rate $\bar{\nu}_e$ for a TEM. Results from the Lorentz collision model are compared with the Sugama model. In the legend, $R^E=0$ means that energy conserving terms are ignored in C^F , $R^M=0$ means that momentum conserving terms are ignored in C^F , and $k_\perp=0$ means all FLR terms are ignored in C^L .

Lorentz model and the Sugama model is due to the inclusion of energy diffusion in the latter. Only when the temperature gradient scale lengths for both species were neglected ($a/L_{Ti}=a/L_{Te}=0$), and the density gradient scale lengths increased ($a/L_{na}=3$) to destabilize the intermediate $k_\theta \rho_s$ TEM, was a small but non-negligible effect seen. This is shown in figure 5 for fixed $\bar{\nu}_e=0.2$. For comparison, results using the simple Lorentz model are also shown in blue. An important result of this scan is to show that for $k_\theta \rho_s < 1.5$, no significant FLR collisional effect on the TEM is observed.

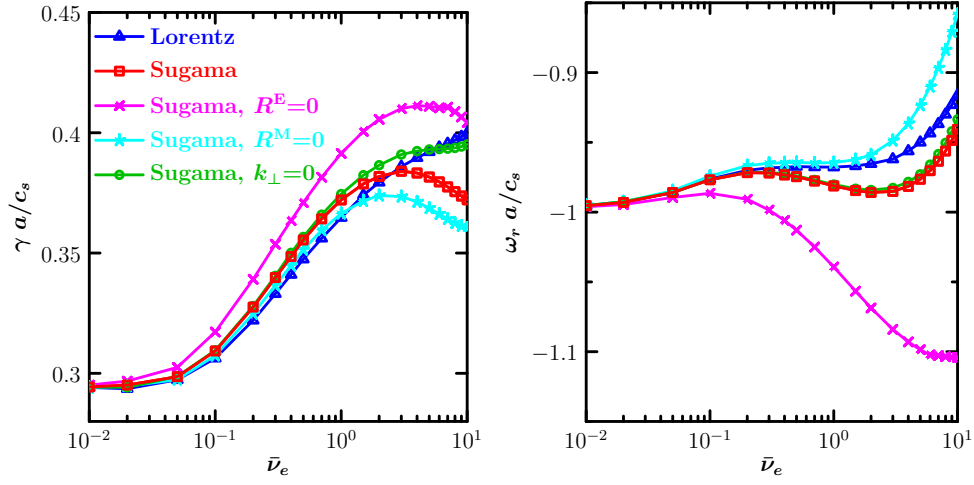


Figure 3. Linear growth rate γ and real frequency ω_r versus collision rate $\bar{\nu}_e$ for a KBM. Results from the Lorentz collision model are compared with the Sugama model. In the legend, $R^E=0$ means that energy conserving terms are ignored in C^F , $R^M=0$ means that momentum conserving terms are ignored in C^F , and $k_\perp=0$ means all FLR terms are ignored in C^L .

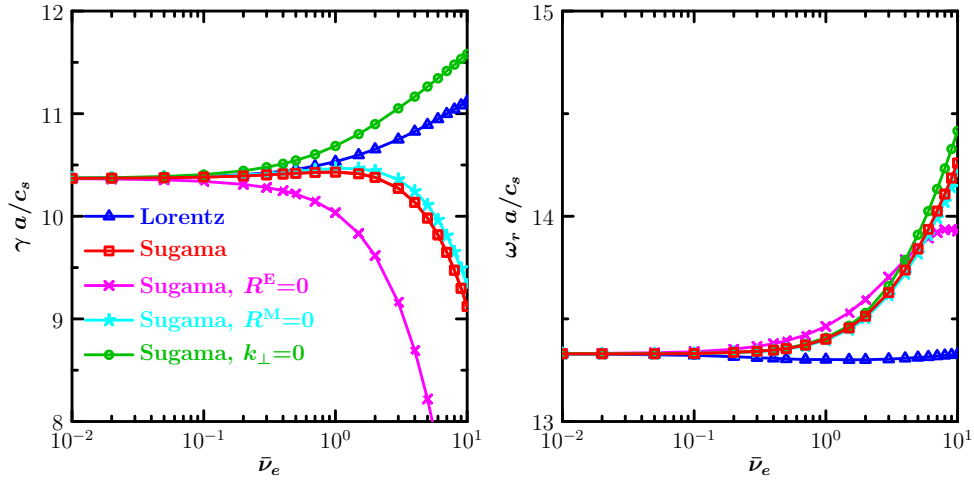


Figure 4. Linear growth rate γ and real frequency ω_r versus collision rate $\bar{\nu}_e$ for an ETG mode. Results from the Lorentz collision model are compared with the Sugama model. In the legend, $R^E=0$ means that energy conserving terms are ignored in C^F , $R^M=0$ means that momentum conserving terms are ignored in C^F , and $k_\perp=0$ means all FLR terms are ignored in C^L .

Note that, in figure 5, a second branch of the TEM appears for $k_\theta = \rho_s > 2$. For this branch, FLR collision terms do enhance the stabilization somewhat, but this result is of questionable importance because the mode is so close to threshold. The added stabilization due to FLR collisional corrections (in the limit of zero temperature gradients) is broadly consistent with results from GS2 [23]. We emphasize, however, that for realistic experimental profiles, our results show that FLR collisional effects are likely negligible for low-to-intermediate $k_\theta \rho_s$ modes.

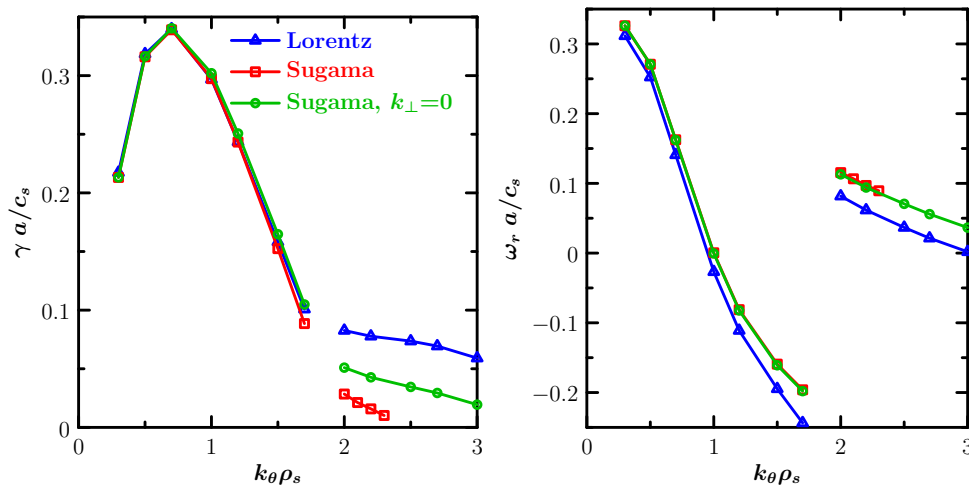


Figure 5. Linear growth rate γ and real frequency ω_r versus wavenumber $k_\theta \rho_s$ for a TEM with zero temperature gradients at $\bar{v}_e=0.2$. Results from the Lorentz collision model are compared with the Sugama model both neglecting and including FLR collision terms. The latter were found to be negligible for cases with finite temperature gradient.

For high- $k_\theta \rho_s$ modes, however, the FLR corrections in the collision operator become important. As shown in figure 4 for the ETG case, for which $k_\theta \rho_s = 18$, the Lorentz component of the collision operator is destabilizing. This is in contrast to the ITG case shown in figure 1. Comparisons between the Sugama model without FLR terms indicates that energy diffusion also has a destabilizing effect (i.e., the green curve increases more rapidly than the blue curve due to energy diffusion). However, inclusion of FLR terms in the Sugama model (red curve) yields a strong stabilizing effect which dominates all other effects. Thus, FLR corrections, which are typically neglected in gyrokinetic codes, will be important for multiscale simulations that couple ion and electron scale physics.

Finally, we examine gyrokinetic linear instabilities in the presence of non-trace impurity fraction. This is an important issue since the fraction of impurities from the wall is expected to be non-negligible in the highly-collisional pedestal. For these simulations, we use the standard ITG case parameters and include fully-stripped carbon impurity ions with $z_I=6$. The impurity equilibrium temperature, and temperature gradient scale length, are set equal to the main ion values. The impurity density gradient scale length, which is determined from quasineutrality, is also set equal to the main ion value. The ion-carbon density ratio is specified through the impurity charge dilution factor, $f_I \doteq z_I n_I / n_e$. Results which compare the Lorentz collision operator with the full Sugama operator, are shown in figure 6. It is clear that the accuracy of the Lorentz model (in comparison to the Sugama operator) decreases as f_I increases, such that the Lorentz model tends to underestimate the growth rate. While the Lorentz model describes only electron collisions (which provide the dominant collisional interaction), the Sugama model additionally describes ion-ion collisions. To assess the role of ion-ion collisions, we show results for a case with adiabatic electrons (no electron collisions)

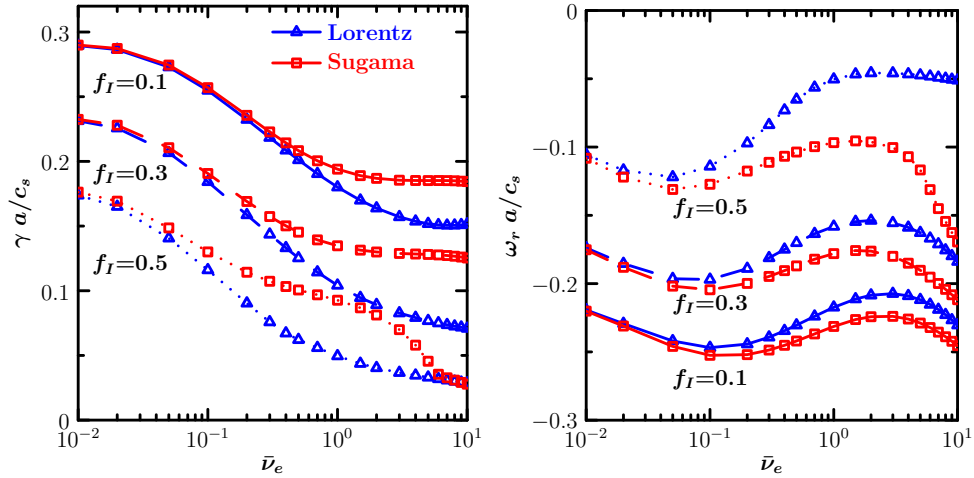


Figure 6. Linear growth rate γ and real frequency ω_r versus collision rate $\bar{\nu}_e$ for an ITG mode with varying carbon impurity fraction f_I . Results from the Lorentz collision model are compared with the Sugama model.

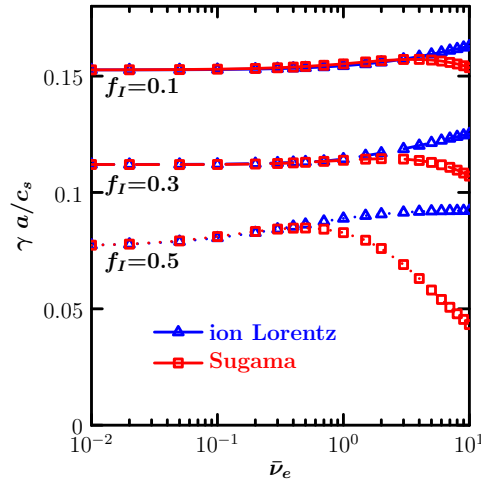


Figure 7. Linear growth rate γ versus collision rate $\bar{\nu}_e$ for an ITG mode with adiabatic electrons and with varying carbon impurity fraction f_I . Results from the ion-ion Lorentz collision model are compared with the Sugama model.

in figure 7. This case shows that ion-ion collisions are stabilizing at large $\bar{\nu}_e$. This effect accounts for the drop in the red curve at large $\bar{\nu}_e$ for $f_I=0.5$ in figure 6. The stabilizing effect of ion-ion collisions on the low- $k_\theta \rho_s$ ITG mode (driven by passing ions) is analogous to the observed stabilization of the high- $k_\theta \rho_s$ ETG mode (driven by passing electrons) due to electron collisions (see figure 4).

3.2. Damping of the residual zonal potential

We have also compared the effect of collision models on the damping of the residual zonal ($k_\theta = 0$) potential. Zonal flows are known to be an important mechanism to regulate ITG turbulence in nonlinear gyrokinetic simulations. The time evolution of the axisymmetric

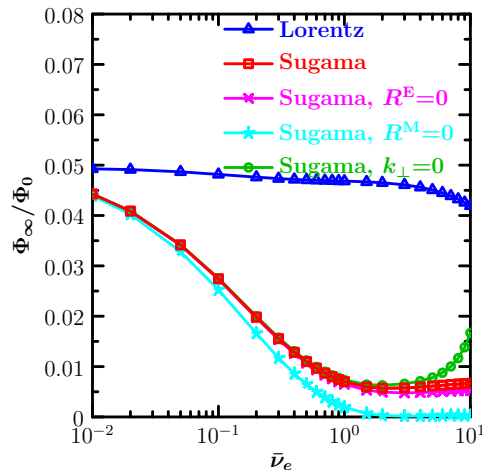


Figure 8. Residual potential versus collision rate $\bar{\nu}_e$. Results from the Lorentz collision model are compared with the Sugama model. In the legend, $R^E=0$ means that energy conserving terms are ignored in C^F , $R^M=0$ means that momentum conserving terms are ignored in C^F , and $k_\perp=0$ means all FLR terms are ignored in C^L .

potential gives rise to decaying oscillations of geodesic acoustic modes (GAMs) with a finite long-time residual value, $\Phi_{t=\infty}/\Phi_{t=0}$. It is well-known from analytic theory [4] that ion-ion collisions can reduce the residual zonal flow. This is demonstrated in figure 8 using the Sugama model. In contrast, for the Lorentz model, only a negligible reduction of the residual zonal flow is observed, since the Lorentz model does not retain ion-ion collisions. Thus, the Lorentz model is not appropriate for accurately modeling the effects of collisions on zonal flows. For the Sugama model, neglecting the energy restoring term gives rise to only a small error in the zonal flow damping. This is in contrast to the result for ITG modes, in which case the energy restoring term cannot be neglected. Also, unlike the ITG case, neglecting the momentum restoring term yields the largest error, overestimating the collisional damping rate, which is in qualitative agreement with the analytic result of Xiao [24].

3.3. Effect of collisions on turbulent fluxes

The impact of collisions and collision models on nonlinear ITG turbulence has also been studied. These simulations use a radial box of length $L_x=89.9\rho_s$ with $N_r=120$ radial modes and a binormal box of length $L_y=114.3\rho_s$ with $N_\alpha=12$ complex toroidal modes. With these choices, we resolve up to $k_\theta\rho_s=0.77$. Other resolutions are $N_\theta=28$, $N_\xi=16$, and $N_u=8$ with $u_{max}^2=8$. The simulations use the same ITG test case parameters with varying carbon impurity fraction f_I as those presented in figure 6. One exception is that the nonlinear simulations are electromagnetic, with small but finite β ($\beta_{e,\text{unit}}=0.05\%$ with $\beta_*=0$). Since CGYRO is an explicit code, finite β acts to reduce the frequency of the kinetic Alfvén wave and thus increase the maximum stable linear timestep. The pure plasma results ($f_I=0$) have previously been benchmarked with GYRO for the Lorentz collision model [5].

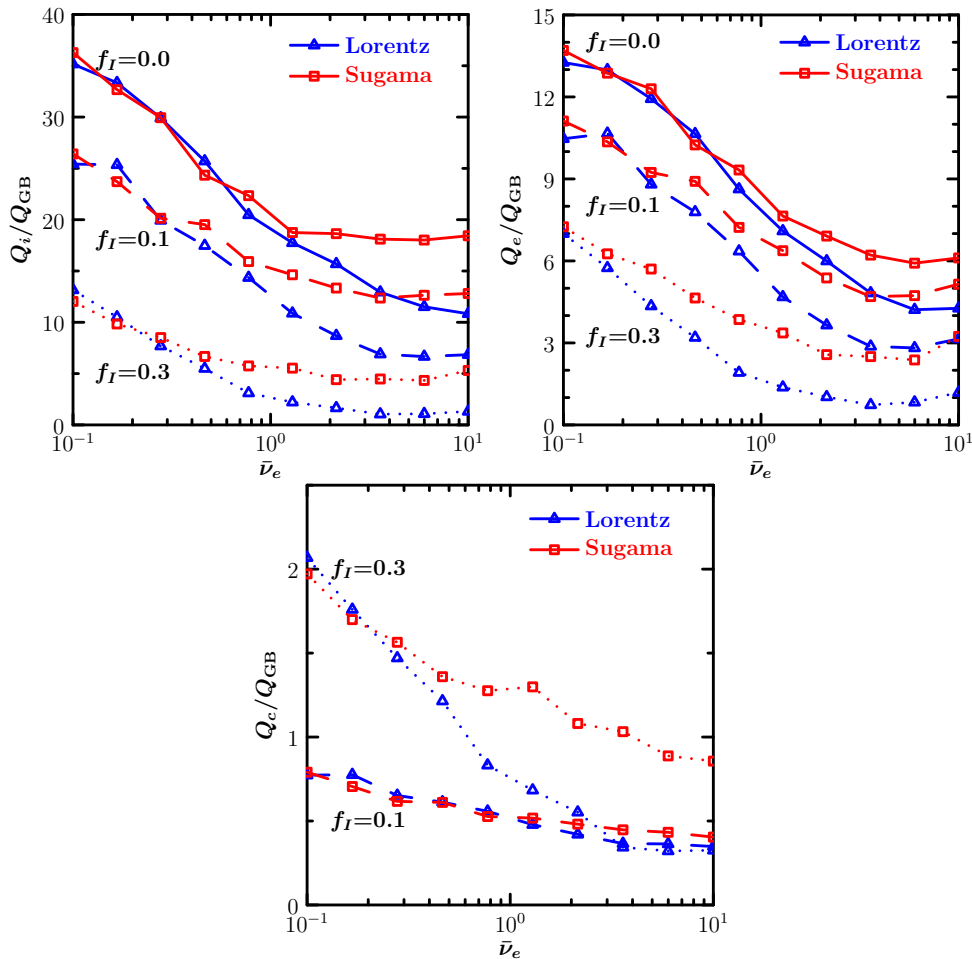


Figure 9. Nonlinear ion, electron, and carbon energy fluxes Q versus collision rate $\bar{\nu}_e$ for an ITG mode with varying carbon impurity fraction f_I . Results from the Lorentz collision model are compared with the Sugama model.

The ion, electron, and carbon energy fluxes are shown in figure 9. As expected, based on the previous linear results, the accuracy of the Lorentz model decreases as $\bar{\nu}_e$ increases. In all cases, the Lorentz model underestimates the energy fluxes for each species. This is consistent with both previous linear results; namely, the Lorentz model underestimates the linear growth rate for finite- $k_\theta \rho_s$ ITG modes (see figure 6) and also underdamps the stabilizing zonal flows (see figure 8). Thus for moderate collision frequency ($\bar{\nu}_e \sim 1$) and moderate impurity fraction ($f_I = 0.3$) – typical of a tokamak pedestal – use of the Lorentz operator can lead to a factor-of-two error in the simulated energy fluxes.

4. Summary

The implications of advanced collision models on gyrokinetic stability have been studied with the new CGYRO code. While electron Lorentz collisions are stabilizing for the ITG mode and TEM, the effect on KBM and ETG modes, while weaker, is slightly

destabilizing. The simple electron Lorentz model, which is standard in gyrokinetics, was compared against the advanced Sugama collision model. The Sugama model includes multi-species collisions, energy diffusion, momentum and energy conservation terms, and is valid at arbitrary wavelength. For simple test cases, the Lorentz model consistently underestimates the growth rate of the ITG mode (and for the KBM up to $\bar{\nu}_e \sim 2$), while it overestimates the growth rate for the TEM. While the inaccuracy in the Lorentz model is relatively small for the ITG mode and KBM (roughly a few percent), when applied to the TEM the error can be as large as 17%. With impurities, the inaccuracy in the ITG linear growth rate with the Lorentz model increases with increasing impurity fraction. Ion-ion collisions, which are neglected in the Lorentz model but are included in the Sugama model, have a stabilizing effect at large $\bar{\nu}_e$. While momentum conservation in the collision model was found to be negligible, neglecting energy conservation leads to an overestimation of the collisional damping. Thus, when including energy diffusion, it is critical that energy conservation is maintained. While FLR collisional terms were found to be insignificant for low-to-intermediate $k_\theta \rho_s$ modes, this was not the case for the ETG mode. For ETG modes, the full Sugama operator with all FLR terms is required to recover the correct trend for $\bar{\nu}_e > 1$. Thus, for multiscale simulations of the pedestal, long wavelength approximations to the collision operator (as typically used in gyrokinetic codes) are inadequate. In addition, the Lorentz model is not appropriate for calculating the damping of residual zonal flows, since it neglects critical ion-ion collision terms. With the Sugama model, the results show that momentum conservation is important, as neglecting it leads to an overestimation of the zonal flow damping rate. Thus, using advanced multi-species collision models may be important for simulating turbulence in the highly-collisional edge.

Acknowledgments

This material is based upon work supported by the U.S. Department of Energy, Office of Science, Office of Fusion Energy Sciences, Theory program, under Award DE-FG02-95ER54309 and by the Edge Simulation Laboratory project under Grant DE-FC02-06ER54873.

References

- [1] Romanelli F and Briguglio S 1990 *Phys. Fluids B* **2** 754
- [2] Song H and Sen A 1993 *Phys. Fluids B* **5** 2806
- [3] Connor J, Hastie R and Helander P 2006 *Plasma Phys. Control. Fusion* **48** 885
- [4] Hinton F and Rosenbluth M 1999 *Plasma Phys. Control. Fusion* **41** A653
- [5] Candy J, Belli E and Bravenec R 2016 *J. Comput. Phys.* **324** 73
- [6] Belli E and Candy J 2008 *Plasma Phys. Control. Fusion* **50** 095010
- [7] Belli E and Candy J 2012 *Plasma Phys. Control. Fusion* **54** 015015
- [8] Barnes M, Abel I, Dorland W, Ernst D, Hammett G, Ricci P, Rogers B, Schekochihin A and Tatsuno T 2009 *Phys. Plasmas* **16** 072107

- [9] Görler T, Lapillonne X, Brunner S, Dannert T, Jenko F, Merz F and Told D 2011 *J. Comput. Phys.* **230** 7053
- [10] Manas P, Camenen Y, Benkadda S, Hornsby W and Peeters A 2015 *Phys. Plasmas* **22** 062302
- [11] Frieman E and Chen L 1982 *Phys. Fluids* **25** 502
- [12] Sugama H and Horton W 1998 *Phys. Plasmas* **5** 2560
- [13] Candy J 2009 *Plasma Phys. Control. Fusion* **51** 105009
- [14] Candy J and Waltz R 2003 *J. Comput. Phys.* **186** 545
- [15] Waltz R and Miller R 1999 *Phys. Plasmas* **6** 4265
- [16] Belli E and Candy J 2010 *Phys. Plasmas* **17** 112314
- [17] Sugama H, Watanabe T H and Nunami M 2009 *Phys. Plasmas* **16** 112503
- [18] Abel I G, Barnes M, Cowley S C, Dorland W and Schekochihin A A 2008 *Phys. Plasmas* **15** 122509
- [19] Rosenbluth M, Ross D and Kostomarov D 1972 *Nucl. Fusion* **12** 3
- [20] Waltz R, Staebler G, Dorland W, Hammett G, Kotschenreuther M and Konings J 1997 *Phys. Plasmas* **4** 2482
- [21] Miller R, Chu M, Greene J, Lin-liu Y and Waltz R 1998 *Phys. Plasmas* **5** 973
- [22] Candy J, Holland C, Waltz R, Fahey M and Belli E 2009 *Phys. Plasmas* **16** 060704
- [23] Ernst D, Basse N, Dorland W, Fiore C, Lin L, Long A, Porkolab M, Zeller K and Zhurovich K 2004 *Proceedings of the 21st IAEA Fusion Energy Conference, Chengdu, China, 2006* TH/1-3
- [24] Xiao Y, Catto P and Molvig K 2007 *Phys. Plasmas* **14** 032302

DISCLAIMER

This report was prepared as an account of work sponsored by an agency of the United States Government. Neither the United States Government nor any agency thereof, nor any of their employees, makes any warranty, express or implied, or assumes any legal liability or responsibility for the accuracy, completeness, or usefulness of any information, apparatus, product, or process disclosed, or represents that its use would not infringe privately owned rights. Reference herein to any specific commercial product, process, or service by trade name, trademark, manufacturer, or otherwise, does not necessarily constitute or imply its endorsement, recommendation, or favoring by the United States Government or any agency thereof. The views and opinions of authors expressed herein do not necessarily state or reflect those of the United States Government or any agency thereof.